Scilight

*Advanced Mechatronics*
https://www.sciltp.com/journals/am


*Article*

# Disturbance Suppression of Dual Three-Phase PMSM Drives Based on Model Predictive Repetitive Control

Le Gao [1,†], Weijun Liu [2,†] and Junxiao Wang [1,*]

[1] Sany Heavy Machinery Company Ltd., Huzhou 215300, China
[2] College of Information Engineering, Zhejiang University of Technology, Hangzhou 310023, China
* Correspondence: wjx2017@zjut.edu.cn
† These authors contributed equally to this work.

**How To Cite**: Gao, L.; Liu, W.; Wang, J. Disturbance Suppression of Dual Three-Phase PMSM Drives Based on Model Predictive Repetitive Control. *Adv. Mechatron.* **2026**, *1*(1), 2.

**Publication History**
Received: 24 May 2026
Revised: 17 June 2026
Accepted: 8 July 2026
Published: 3 August 2026

**Abstract:** For the dual three-phase permanent magnet synchronous motor (DTP-PMSM) drive system, periodic harmonic disturbances and non-periodic disturbances always exist, severely impacting system performance. In this article, the impacts of different types of disturbances on the DTP-PMSM control system are first analyzed. Subsequently, based on the internal model principle (IMP), a model predictive repetitive control (MPRC) strategy is proposed to effectively suppress periodic harmonic disturbances of specific orders in the system. Moreover, to mitigate the impact of non-periodic disturbances on MPRC, an improved equivalent input disturbance (IEID) method is introduced. Considering the phase lag issue associated with IEID, a corresponding phase compensation method (PC-IEID) is designed to enhance compensation accuracy. Finally, the effectiveness of the proposed methods is verified through comparative experiments.

**Keywords:** dual three-phase permanent magnet synchronous motor (DTP-PMSM); model predictive repetitive control (MPRC); internal model principle (IMP); improved equivalent input disturbance (IEID)

## 1. Introduction

In recent years, multi-phase permanent magnet synchronous motors (PMSMs) have gained extensive applications owing to their unique structural advantages, among which the dual three-phase permanent magnet synchronous motor (DTP-PMSM) with two sets of isolated three-phase windings is most representative [1]. Such a structure provides outstanding fault tolerance through physical winding isolation. Benefiting from high control flexibility, low-voltage and high-power capability [2, 3], DTP-PMSMs have been widely used in electric aircraft, electric vehicles, and other high-performance fields.

However, this winding configuration also leads to distinctive electromagnetic characteristics. Compared with conventional three-phase motors, DTP-PMSMs feature smaller stator leakage inductance, so even slight voltage fluctuations in the control loop can induce significant stator harmonic current disturbances. These harmonics not only increase copper losses [4] but also aggravate mechanical vibration, thus undermining their inherent low-torque-ripple advantage. Therefore, effective suppression of harmonic disturbances has become critical to further improving the performance of DTP-PMSM drives.

To address the harmonic disturbance issue in DTP-PMSMs, vector space decomposition (VSD) theory has been widely adopted [5]. This approach decouples system harmonics into the $z_1$-$z_2$ subspace and enables independent harmonic suppression. Existing periodic harmonic mitigation strategies mainly focus on two aspects: inverter modulation design and advanced control algorithms.

Modulation-based methods focus on reducing the voltage vector amplitude in the $z_1$-$z_2$ subspace [6]. The four-vector space vector pulse width modulation (SVPWM) scheme maximizes the voltage vector amplitude in the $\alpha$-$\beta$ subspace while minimizing that in the $z_1$-$z_2$ subspace [7], but it increases implementation complexity and introduces a tradeoff between modulation depth and control performance. Dual three-phase SVPWM simplifies implementation, but its harmonic suppression capability is still insufficient, calling for more advanced control methods.

In the field of control algorithms, model predictive control (MPC) has been widely used in DTP-PMSM drives due to its fast current response, few tuning parameters, and multi-constraint handling capability [8]. MPC is divided into finite control set MPC (FCS-MPC) and continuous control set MPC (CCS-MPC).

In [9–11], FCS-MPC selects limited voltage vectors to maximize $\alpha$-$\beta$ subspace vector amplitude and minimize $z_1$-$z_2$ subspace currents, effectively suppressing low-order harmonics. However, limited candidate vectors cause quantization errors, poor modulation flexibility, and discontinuous switching states, requiring additional optimization.

To overcome these drawbacks and directly generate the optimal voltage vector, CCS-MPC has been developed, which retains the cost function design and model predictive characteristics of FCS-MPC while realizing arbitrary voltage vector synthesis [12]. However, the performance of MPC relies heavily on model accuracy. Unmodeled periodic disturbances and parameter mismatches will seriously degrade the control performance. Thus, it is essential to compensate for both periodic harmonics and parameter uncertainties in MPC-based DTP-PMSM drives.

On one hand, harmonics and parameter mismatches are treated as lumped disturbances, estimated by observers and compensated feedforwardly. In [13], extended state observer (ESO) estimates lumped disturbances but suffers from bandwidth tradeoff between noise suppression and estimation accuracy. An improved ESO embedded with disturbance internal model is proposed in [14] to enhance observation accuracy, yet it requires more memory. The equivalent input disturbance (EID) method suppresses lumped disturbances and measurement noise [15], but inherent observer-estimator coupling weakens high-frequency compensation. Improved EID (IEID) eliminates this coupling [16], yet its low-pass filter introduces phase lag. IEID observer (IEIDO) handles time-varying disturbances but still suffers from phase lag limitation [17]. Other observers including generalized proportional integral observer (GPIO) [18] and disturbance observer (DOB) [19] also enhance system robustness. In addition, Momir Stanković et al. proposed the resonant extended state observer (RESO) to suppress periodic harmonics, yet it is susceptible to frequency drift and fails to address parameter-induced non-periodic disturbances [20].

On the other hand, based on the internal model principle (IMP), embedding the internal model of periodic disturbances into the control loop can achieve accurate rejection. Typical methods include resonant controllers [21] and repetitive controllers (RC) [22, 23]. RC is often combined with active disturbance rejection control (ADRC) to mitigate current disturbances. In [24,25], repetitive predictive control (RPC) embeds periodic signal internal model into the predictive framework to effectively compensate periodic fluctuations. However, when periodic and aperiodic disturbances coexist, RC performance degrades significantly as aperiodic components interfere with the internal model mechanism.

To overcome the above limitations, this paper analyzes the dominant $6k \pm 1$-order harmonics in DTP-PMSM drives and proposes a MPRC method based on IMP. Since MPRC is designed mainly for periodic disturbances, aperiodic disturbances caused by model mismatches and parameter variations will still degrade its performance. Therefore, a phase-compensated improved equivalent input disturbance (PC-IEID) method is proposed to suppress aperiodic disturbances. The proposed method solves the phase lag problem in conventional IEID and significantly improves the accuracy of aperiodic disturbance compensation, thereby enhancing the robustness and steady-state accuracy of MPRC. The effectiveness of the proposed MPRC+PC-IEID scheme is verified by comparative experiments. The DTP-PMSM drive system studied in this article is shown in Figure 1.

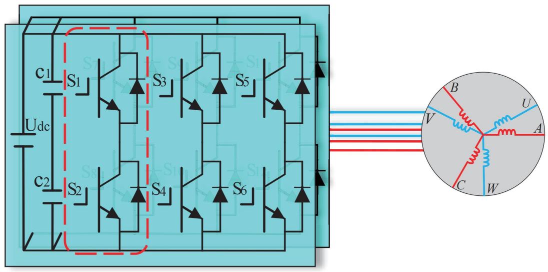


**Figure 1.** Structure of voltage source inverter fed DTP-PMSM.

## 2. Materials and Methods

### 2.1. Traditional Incremental Predictive Model

Within the MPC framework, the predictive model for the DTP-PMSM is obtained from its discrete-time mathematical model. This model predicts the future states based on the current system state and the applied control inputs. Through VSD transformation, the mathematical model of the DTP-PMSM is obtained as

$$\begin{cases} u_d = R_s i_d + L_d \dfrac{di_d}{dt} - \omega_e L_q i_q \\ u_q = R_s i_q + L_q \dfrac{di_q}{dt} + \omega_e L_d i_d + \omega_e \psi_f \\ u_{z1} = R_s i_{z1} + L_z \dfrac{d}{dt} i_{z1} \\ u_{z2} = R_s i_{z2} + L_z \dfrac{d}{dt} i_{z2}. \end{cases} \tag{1}$$

By discretizing the continuous-time state-space Equation (1) via the forward Euler method, the discrete-time dynamic equations of the DTP-PMSM can be expressed as

$$\begin{cases} i_d(k+1) &= \left(1 - \frac{R_s}{L_s} T_s\right) i_d(k) + \omega_e T_s\, i_q(k) + \frac{T_s}{L_s} u_d(k) \\ i_q(k+1) &= -\omega_e T_s\, i_d(k) + \left(1 - \frac{R_s}{L_s} T_s\right) i_q(k) \\ & \quad + \frac{T_s}{L_s} u_q(k) - \frac{\omega_e \psi_f}{L_s} T_s \\ i_{z1}(k+1) &= \left(1 - \frac{R_s}{L_z} T_s\right) i_{z1}(k) + \frac{T_s}{L_z} u_{z1}(k) \\ i_{z2}(k+1) &= \left(1 - \frac{R_s}{L_z} T_s\right) i_{z2}(k) + \frac{T_s}{L_z} u_{z2}(k). \end{cases} \tag{2}$$

These equations can be rewritten in the compact state-space form

$$\begin{cases} x(k+1) = A_{m0} x(k) + B_{m0} u(k) + d(k) \\ y(k) = C x(k), \end{cases} \tag{3}$$

where the state vector $x = [i_d,\ i_q,\ i_{z1},\ i_{z2}]^{\mathrm{T}}$, input $u = [u_d,\ u_q,\ u_{z1},\ u_{z2}]^{\mathrm{T}}$, output $y = x$ ($C = I_4$), and the nominal system matrices are

$$A_{m0} = \begin{bmatrix} 1-\frac{R_s}{L_s}T_s & \omega_e T_s & 0 & 0 \\ -\omega_e T_s & 1-\frac{R_s}{L_s}T_s & 0 & 0 \\ 0 & 0 & 1-\frac{R_s}{L_z}T_s & 0 \\ 0 & 0 & 0 & 1-\frac{R_s}{L_z}T_s \end{bmatrix},$$

$$B_{m0} = \mathrm{diag}\left(\frac{T_s}{L_s}, \frac{T_s}{L_s}, \frac{T_s}{L_z}, \frac{T_s}{L_z}\right),$$

and $d(k) = \begin{bmatrix} 0 & -\frac{\omega_e \psi_f}{L_s}T_s & 0 & 0 \end{bmatrix}^{\mathrm{T}}$.

Based on the prediction Equation (3), the predicted value at time $k$ can be obtained as

$$x(k) = A_{m0}x(k-1) + B_{m0}u(k-1) + d(k-1). \tag{4}$$

By subtracting Equation (4) from Equation (3), the incremental output for time $k+1$ can be expressed as

$$\begin{aligned} \Delta x(k+1) &= x(k+1) - x(k) \\ &= A_{m0}\Delta x(k) + B_{m0}\Delta u(k) + \Delta d(k). \end{aligned} \tag{5}$$

According to Equation (5), even with an incremental formulation, parameter variations can still introduce prediction errors through the term $\Delta d(k)$. Therefore, the multi-dimensional incremental MPC is formulated by augmenting the state with the incremental state

$$\begin{cases} \underbrace{\begin{bmatrix} x(k+1) \\ \Delta x(k+1) \end{bmatrix}}_{x_m(k+1)} = \underbrace{\begin{bmatrix} A_{m0} & \mathbf{0}_4 \\ CA_{m0} & \mathbf{I}_4 \end{bmatrix}}_{A_m} \underbrace{\begin{bmatrix} x(k) \\ \Delta x(k) \end{bmatrix}}_{x_m(k)} + \underbrace{\begin{bmatrix} B_{m0} \\ CB_{m0} \end{bmatrix}}_{B_m} \Delta u(k) \\ \qquad + \underbrace{\begin{bmatrix} \mathbf{I}_4 \\ \mathbf{I}_4 \end{bmatrix}}_{D_m} \Delta d(k) \\ y(k) = \underbrace{\begin{bmatrix} \mathbf{C} & 0 \end{bmatrix}}_{C_m} \begin{bmatrix} x(k) \\ \Delta x(k) \end{bmatrix}. \end{cases} \tag{6}$$

Thus the augmented system is compactly written as $x_m(k+1) = A_m x_m(k) + B_m \Delta u(k) + D_m \Delta d(k)$, $y(k) = C_m x_m(k)$. Based on this model, the output over a prediction horizon $N_p$ with a control horizon $N_c$ can be extrapolated as

$$\mathbf{Y} = \Gamma\, x_m(k) + \Phi\, \mathbf{U} + E\, \mathbf{D}, \tag{7}$$

where

$$\mathbf{Y} = \begin{bmatrix} y(k+1) \\ y(k+2) \\ \vdots \\ y(k+N_p) \end{bmatrix}, \Gamma = \begin{bmatrix} C_m A_m \\ C_m A_m^2 \\ \vdots \\ C_m A_m^{N_p} \end{bmatrix},$$

$$\mathbf{U} = \begin{bmatrix} \Delta u(k) \\ \Delta u(k+1) \\ \vdots \\ \Delta u(k+N_p-1) \end{bmatrix}, \mathbf{D} = \begin{bmatrix} \Delta d(k) \\ \Delta d(k+1) \\ \vdots \\ \Delta d(k+N_p-1) \end{bmatrix},$$

$$\Phi = \begin{bmatrix} C_m B_m & 0 & \cdots & 0 \\ C_m A_m B_m & C_m B_m & \cdots & 0 \\ \vdots & \vdots & \ddots & \vdots \\ C_m A_m^{N_p-1} B_m & C_m A_m^{N_p-2} B_m & \cdots & C_m A_m^{N_p-N_c} B_m \end{bmatrix},$$

and the matrix $E$ has the same structure as $\Phi$, with $B_m$ replaced by $D_m$.

To balance tracking performance and control effort, the cost function is defined as

$$\min_{\mathbf{U}} J = (\mathbf{Y}^{\mathrm{ref}} - \mathbf{Y})^{\mathrm{T}} \mathbf{Q} (\mathbf{Y}^{\mathrm{ref}} - \mathbf{Y}) + \mathbf{U}^{\mathrm{T}} \mathbf{R} \mathbf{U}, \tag{8}$$

where

$$\mathbf{Y}^{\mathrm{ref}} = \begin{bmatrix} y^{\mathrm{ref}}(k+1) & y^{\mathrm{ref}}(k+2) & \cdots & y^{\mathrm{ref}}(k+N_p) \end{bmatrix}^{\mathrm{T}},$$

$$\mathbf{Q} = \mathrm{diag}(Q_1, Q_2, \ldots, Q_{N_p}), \quad \mathbf{R} = \mathrm{diag}(R_1, R_2, \ldots, R_{N_p}).$$

According to quadratic programming theory, the optimal control sequence is

$$\mathbf{U} = (\Phi^{\mathrm{T}} \mathbf{Q} \Phi + \mathbf{R})^{-1} \Phi^{\mathrm{T}} \mathbf{Q} \left[ \mathbf{Y}^{\mathrm{ref}} - \Gamma x_m(k) - E\mathbf{D} \right]. \tag{9}$$

According to receding horizon optimization, only the first control move is applied. The reference voltages for all four axes are

$$\begin{bmatrix} u_d^{\mathrm{ref}}(k) & u_q^{\mathrm{ref}}(k) & u_{z1}^{\mathrm{ref}}(k) & u_{z2}^{\mathrm{ref}}(k) \end{bmatrix}^{\mathrm{T}} = \frac{1}{1-z^{-1}} W \mathbf{U}, \tag{10}$$

where

$$W = \begin{bmatrix} 1 & 0 & 0 & 0 & \cdots & 0 \\ 0 & 1 & 0 & 0 & \cdots & 0 \\ 0 & 0 & 1 & 0 & \cdots & 0 \\ 0 & 0 & 0 & 1 & \cdots & 0 \end{bmatrix}_{4 \times 4N_p}.$$

As shown in Equations (9) and (10), the incremental predictive model effectively mitigates the impact of slowly varying parameters through the integral action and receding-horizon optimization. However, when unmodeled periodic disturbances are present, the disturbance dynamics are not explicitly characterized, leading to accumulation of multi-step prediction errors and steady-state tracking errors as the prediction horizon extends. Therefore, to enhance control performance, a MPRC method is proposed to actively suppress the effects of periodic disturbances.

### 2.2. Disturbance Types and Analysis

For DTP-PMSM, the disturbances in the current loop can be categorized into non-periodic disturbances and periodic harmonic disturbances. Non-periodic disturbances are primarily caused by parameter variation. Periodic harmonic disturbances are generated by stator magnetomotive force (MMF) harmonics, PM flux linkage harmonics and dead-time effects of voltage source inverter.

#### 2.2.1. Periodic Harmonic Disturbance

Stator MMF harmonics mainly originate from the fractional-slot winding structure commonly adopted in DTP-PMSMs. Theoretical modeling usually assumes ideal sinusoidal stator MMF distribution, but practical fractional-slot windings inevitably produce significant spatial harmonics [26], which induce high eddy current losses in permanent magnets [27], increasing PM temperature and causing parameter variations as speed rises. Although optimized designs such as stator slot skewing mitigate harmonic MMF [28], residual harmonics still exist.

PM flux linkage harmonics, caused by stator slotting effects and manufacturing limitations, are another major source of periodic disturbances and are generally unavoidable. Under symmetric loading conditions, these non-sinusoidal flux components are uniformly distributed across phase windings and introduce periodic harmonic disturbances in stator currents during motor rotation.

As shown in Figure 2, the inverter dead-time introduced to prevent shoot-through also generates harmonic voltages. While dead-time compensation can precisely suppress certain harmonics [29], residual harmonic components still remain in the system.

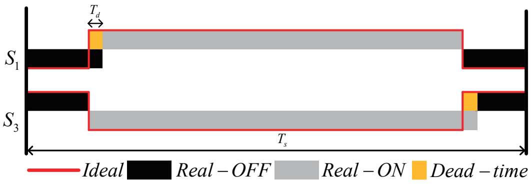


**Figure 2.** Principle of inverter PWM dead-time.

After VSD transformation, dominant periodic harmonics concentrate in the $z_1$-$z_2$ subspace, mainly $6k \pm 1$-order harmonics ($k = 1, 2, 3, \dots$). These harmonic currents do not participate in electromagnetic energy conversion but increase copper losses, cause vibration and noise, and undermine DTP-PMSM's low-torque-ripple advantage. Meanwhile, harmonics in the $d$-$q$ subspace produce 12th-order torque pulsations, further degrading system performance.

#### 2.2.2. Non-Periodic Disturbances

Non-periodic disturbances are primarily caused by parameter mismatches between the actual system and the nominal model used in controller design, including variations in stator resistance $R_s$, d-axis inductance $L_d$, q-axis inductance $L_q$ and leakage inductance $L_z$. Theoretical analysis shows that the influence of stator resistance variation on system performance is negligible, while even small changes in inductance will lead to significant prediction errors in the model predictive control (MPC) framework. These non-periodic disturbances exist in both the $d$-$q$ fundamental subspace and the $z_1$-$z_2$ harmonic subspace, which will degrade the periodic disturbance suppression performance of the repetitive controller and even threaten system stability.

### 2.3. Controller and Observer Design

#### 2.3.1. MPRC Controller Design

The z-domain transfer function of the conventional repetitive controller (CRC) can be expressed as

$$G_{crc}(z) = k_{rc}\frac{Q(z)z^{-N+Comp}}{1 - Q(z)z^{-N}}, \tag{11}$$

where $N = \frac{T_h}{T_s}$, $T_h = \frac{2\pi}{\omega_h}$, $\omega_h$ is the frequency of the harmonic that needs to be suppressed, Comp is for phase compensation, $k_{rc}$ is the controller gain, and $Q(z)$ typically chooses a constant less than 1 or a low-pass filter to enhance system stability.

However, CRC requires memory to store full-period data (N sampling steps), slowing convergence especially for long periods. To improve transient performance and convergence speed, an $nk \pm m$-order repetitive controller is proposed in [21] to handle specific subharmonics, with its digital transfer function as

$$G_{rc}(z) = k_{rc}\frac{cos\left(\frac{2\pi m}{n}\right)z^{-N/n} - 1}{z^{-2N/n} - 2cos\left(\frac{2\pi m}{n}\right)z^{-N/n} + 1}. \tag{12}$$

From the analysis of the previous section, to suppress the harmonics in the harmonic space, $n = 6$ and $m = 1$ are taken. To ensure the stability and robustness of the system, a low-pass filter $Q(z)$ and a phase compensation filter $G_f(z)$ are required. Thus, the improved digital $6k \pm 1$ RC is shown in Equation (13).

$$G_{rc}(z) = k_{rc}\frac{(Q(z)/2)z^{-N/6} - Q^2(z)}{z^{-N/3} - Q(z)z^{-N/6} + Q^2(z)}G_f(z). \tag{13}$$

The structure of the designed predictive repetitive controller is shown in Figure 3.

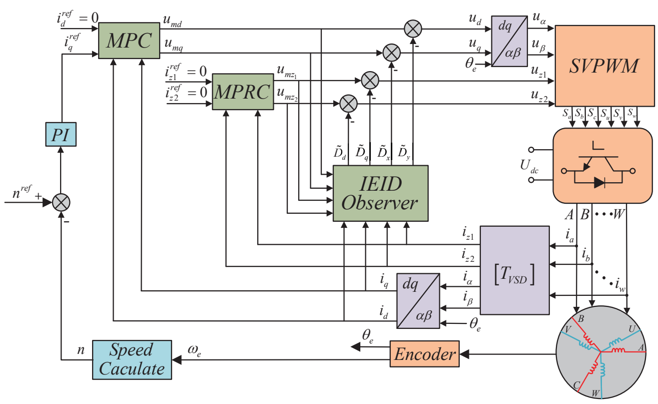


**Figure 3.** Proposed MPRC control strategy for DTP-PMSM.

It can be seen that embedding the $G_{rc}$ controller is equivalent to applying $(1+G_{rc}(z))^{-1}$ to both sides of the incremental model, as shown in Equation (14).

$$\begin{aligned}&(1 + G_{rc}(z))^{-1}x_m(k + 1)\\ &= A_m(1 + G_{rc}(z))^{-1}x_m(k) + B_m(1 + G_{rc}(z))^{-1}\Delta u(k).\end{aligned} \tag{14}$$

The Bode plot of the transfer function $(1 + G_{rc}(z))^{-1}$ is shown in Figure 4.

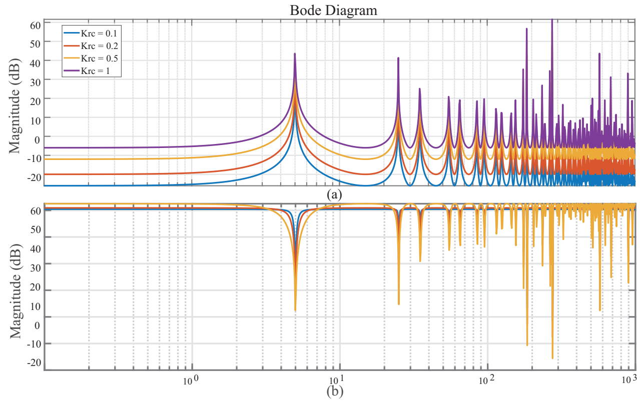


**Figure 4.** Bode plots of (**a**)$G_{rc}(z)$ and (**b**)$(1+G_{rc}(z))^{-1}$.

When the parameters are properly selected, it provides significant gain only at the resonant frequency, with almost no impact at other frequencies. Apart from the resonant frequency, the amplitude and phase of the system remain virtually unchanged. Therefore, the above equation can be written as

$$x_m(k+1) = A_{m0}x_m(k) + B_{m0}\left(1+G_{rc}(z)\right)^{-1}\Delta u(k). \quad (15)$$

Since the $z_1$-$z_2$ space contains harmonics of various orders and has a significant impact on the system, the MPRC controller is applied exclusively to the $z_1$-$z_2$ space. After embedding the repetitive controller, the control input of the system is given by

$$u_m(k) = \left(1+G_{rc}(z)\right)u^{ref}(k). \quad (16)$$

RC achieves periodic disturbance rejection by storing historical disturbance information through a delay-chain. However, in the presence of non-periodic disturbances, the periodic matching mechanism becomes ineffective, resulting in a mismatch between stored and real-time disturbance frequencies and causing delayed compensation. In addition, non-periodic components generate secondary harmonics, which further compromise system stability. From the analysis in the previous section, both spaces contain non-periodic disturbances caused by parameter changes. Therefore, to improve the precision of the MPRC, it is necessary to effectively suppress the nonperiodic disturbances in the system.

### 2.3.2. PC-IEID Observer Design

The proposed MPRC effectively suppresses $6k \pm 1$-order periodic harmonic disturbances, but its inherent periodic matching mechanism makes it vulnerable to non-periodic disturbances such as parameter mismatches and load mutations, which will degrade control accuracy and even affect system stability. Therefore, this paper introduces a PC-IEID observer to estimate and compensate non-periodic disturbances, further enhancing the robustness of the composite control scheme.

For the discrete state-space model of the DTP-PMSM system, the system state includes $d$-$q$ axis and $z_1$-$z_2$ axis currents, the input is the inverter output voltage, and the output is the measured value of each axis current. To estimate the state variables of the system, a full-dimensional state observer is first constructed, and the state estimate is updated in real time using the input and output information of the system. The observer corrects the state estimate by introducing an output error feedback term. By reasonably designing the observer gain matrix, the state estimation error can be quickly converged to zero. The mathematical expression of the full-dimensional state observer is

$$\begin{cases} \hat{x}(k+1) = A_{m0}\hat{x}(k) + B_{m0}u_m(k) + L(y(k)-\hat{y}(k)) \\ \hat{y}(k) = C\hat{x}(k), \end{cases} \quad (17)$$

where $\hat{x}(k)$ and $\hat{y}(k)$ are the estimated values of the state and output, respectively; $A_{m0}$, $B_{m0}$, and $C$ are the nominal state matrix, input matrix, and output matrix of the system, respectively; $u_m(k)$ is the control quantity output by the MPRC controller; $L$ is the observer gain matrix, which is used to adjust the convergence speed and anti-noise ability of the observer. Define the state estimation error as $\Delta x(k) = x(k) - \hat{x}(k)$. When the observer gain is designed reasonably, this error will asymptotically converge to zero.

According to the equivalent input disturbance principle, all system disturbances can be equated to a disturbance signal on the control input. The preliminary equivalent input disturbance is derived based on state estimation error. Since the input matrix is usually non-square and cannot be directly inverted, the Moore-Penrose pseudoinverse is used to obtain the unique least squares solution. The preliminary estimation formula is

$$\hat{d}_e(k) = B^{+}LC\Delta x(k) + u_m(k) - u(k), \quad (18)$$

where $B^{+} = (B_{m0}^{T}B_{m0})^{-1}B_{m0}^{T}$ is the pseudoinverse of the input matrix $B_{m0}$; $u(k)$ is the control quantity finally applied to the system.

The preliminary estimated disturbance contains high-frequency measurement noise and high-order harmonic components. Direct feedforward compensation will reintroduce these interferences and degrade control performance. Therefore, a first-order low-pass filter is adopted to retain low-frequency main disturbances and filter out high-frequency noise, featuring simple structure and low computational cost for real-time control. Its discrete-domain transfer function is

$$F(z) = \frac{1+z^{-1}}{(1+\alpha)+(1-\alpha)z^{-1}}, \quad (19)$$

where $\alpha = \frac{2T}{T_s}$, $T$ is a parameter related to the cutoff frequency of the low-pass filter, and $T_s$ is the system sampling period. The filtered disturbance estimate $\tilde{d}_e(k)$ satisfies $\tilde{D}_e(z) = F(z)\hat{D}_e(z)$, where $\tilde{D}_e(z)$ and $\hat{D}_e(z)$ are the $z$-transforms of $\tilde{d}_e(k)$ and $\hat{d}_e(k)$, respectively. The final composite control law adopts a feedforward compensation structure, which cancels the filtered equivalent input disturbance from the control quantity output by the MPRC, thereby eliminating the impact of non-periodic disturbances on the system

$$u(k) = u_m(k) - \tilde{d}_e(k). \quad (20)$$

Compared with the traditional EID method, the IEID method removes the constraint relationship between the observer and the estimator by reconstructing the transfer function of disturbance estimation, and its equivalent disturbance estimation can be expressed in a more general form $\tilde{D}_e(z) =$

$H(z)B^{+}LC\Delta X(z)$, where $H(z)$ is the transfer function to be designed. When $H(z) = F(z)[1 - F(z)]^{-1}$, the IEID method is completely equivalent to the traditional EID method. By flexibly designing $H(z)$, the IEID method can obtain better disturbance estimation performance than the traditional EID.

However, the low-pass filter in IEID still introduces phase lag in disturbance estimation. The phase lag becomes significant when disturbance frequency approaches the filter cutoff frequency, leading to inaccurate feedforward compensation and degraded MPRC accuracy, especially under medium and high speed conditions. To solve this problem, this paper proposes a phase-locked loop (PLL) based phase compensation strategy, adding a phase compensation link to the IEID observer to form PC-IEID.

As shown in Figure 5, Figure 5a is the structure of the phase compensation unit, and the overall equivalent structure of the PC-IEID is shown in Figure 5b. This strategy adopts a PLL structure to realize static-free tracking of input disturbance signals and obtain real-time frequency and phase information of disturbances. A first-order all-pass filter is introduced in the feedback loop for lead phase compensation to offset the lag phase introduced by the low-pass filter. By tuning the parameters of the all-pass filter, the phase lag of the low-pass filter at the cutoff frequency can be accurately compensated, thereby improving the estimation accuracy of non-periodic disturbances.

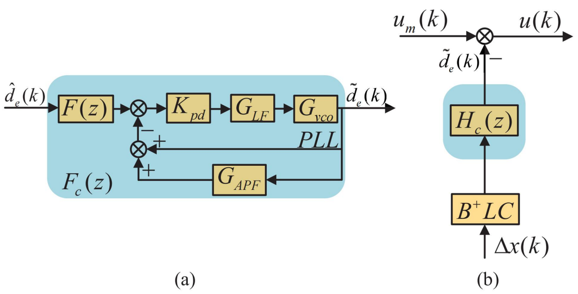


**Figure 5.** The structure of phase-compensated (**a**) and equivalent PC-IEID (**b**).

PC-IEID includes four core components, namely phase detector, loop filter, voltage-controlled oscillator and all-pass filter, with their transfer functions presented as follows:

$$\begin{cases} K_{pd} = 1, \quad G_{LF}(s) = k_p + \dfrac{k_i}{s}, \\ G_{vco}(s) = \dfrac{K_{vco}}{s}, \quad G_{APF}(s) = k\dfrac{\tau s + 1}{s + 1}, \end{cases} \tag{21}$$

where $K_{pd}$ denotes the gain of the phase detector, $G_{LF}(s)$ the proportional-integral loop filter with coefficients $k_p$ and $k_i$, $G_{vco}(s)$ the transfer function of the voltage-controlled oscillator, and $G_{APF}(s)$ the first-order all-pass filter with gain $k$ and time constant $\tau$ for phase compensation. Figure 6 presents Bode plots of $F(s)$, $H(s)$, and $H_c(s)$. The low-pass filter cutoff frequency is set to 100 rad/s to balance harmonic suppression and low-frequency phase lag. The compensated system features a slightly higher cutoff frequency, which hardly impairs harmonic filtering but greatly reduces low-frequency phase lag and improves disturbance estimation accuracy.

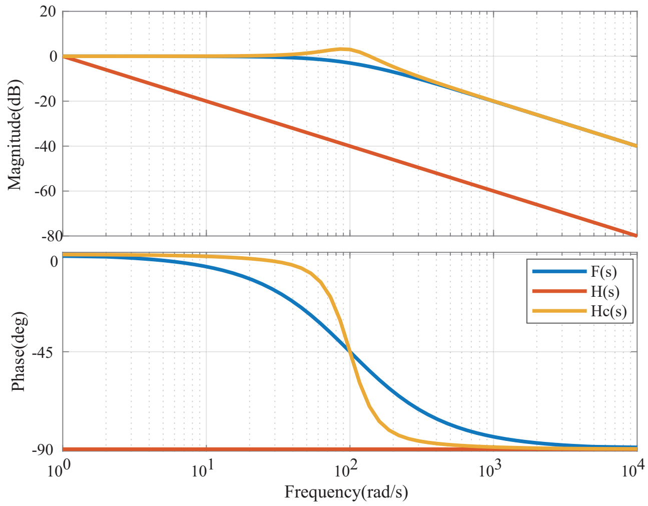


**Figure 6.** Bode diagram of the $F(s)$, $H(s)$ and $H_c(s)$.

PC-IEID parameter tuning includes three main steps. First, tune PLL parameters to ensure fast and accurate disturbance tracking. Second, insert a first-order all-pass filter in the PLL feedback loop for lead compensation. Third, adjust its time constant and gain to make the lead phase exactly cancel the low-pass filter lag at the cutoff frequency, achieving nearly phase-shift-free disturbance estimation. After compensation, the equivalent input disturbance estimation formula is rewritten from the traditional IEID form as

$$\tilde{d}_e(k) = H_c(z)B^{+}LC\Delta x(k), \tag{22}$$

where $H_c(z) = F_c(z)[1 - F_c(z)]^{-1}$ is the compensated transfer function. Sufficient low-frequency gain ensures the estimate approximates the true disturbance. The control law retains the traditional IEID feedforward structure, maintaining non-periodic disturbance suppression while eliminating phase lag and enhancing MPRC accuracy and robustness.

The proportional-integral loop filter of the PLL is designed according to the desired tracking bandwidth and damping ratio. Since the phase detector gain is $K_{pd}$ and the VCO gain is $K_{vco}$, the closed-loop characteristic equation of the second-order PLL can be written as

$$s^2 + K_{pd}K_{vco}k_p s + K_{pd}K_{vco}k_i = 0. \tag{23}$$

By assigning the desired natural frequency $\omega_n$ and damping ratio $\zeta$, the loop-filter parameters are selected as

$$k_p = \frac{2\zeta\omega_n}{K_{pd}K_{vco}}, k_i = \frac{\omega_n^2}{K_{pd}K_{vco}}. \tag{24}$$

In this study, $K_{pd} = 1$ and $K_{vco} = 1$ are adopted. The damping ratio is generally selected as $\zeta = 0.707$ to obtain a compromise between fast tracking and overshoot suppression. The PLL bandwidth should be lower than the sampling frequency and sufficiently separated from high-frequency noise. Therefore, $\omega_n$ is selected within $0 < \omega_n < 0.1\frac{\pi}{T_s}$. A larger $\omega_n$ improves the frequency tracking speed during speed transients, but may amplify measurement noise and deteriorate the disturbance estimation accuracy.

For the all-pass filter $G_{APF}(s) = k\dfrac{\tau s + 1}{s + 1}$, the gain $k$ is fixed to 1 in this study to avoid additional amplitude scaling during phase compensation. The time constant $\tau$ is used to tune the phase compensation provided by the filter. Since the low-pass filter introduces a phase lag around the cutoff angular frequency $\omega_0$, $\tau$ is selected so that the phase of $G_{APF}(s)$ at $\omega_0$ approximately cancels this lag.

At the design frequency $\omega_0$, the phase of $G_{APF}(s)$ can be expressed as

$$\phi_{APF}(\omega_0) = \arctan(\tau\omega_0) - \arctan(\omega_0). \tag{25}$$

The desired compensation phase $\phi_c$ is obtained from the Bode plot of the disturbance estimation filter. Therefore, $\tau$ is tuned such that

$$\phi_{APF}(\omega_0) \approx \phi_c. \tag{26}$$

In practical implementation, $\tau$ is adjusted iteratively and verified by the Bode response until the phase lag of the low-pass filter around $\omega_0$ is sufficiently compensated. A smaller $\tau$ provides limited phase compensation, so the disturbance estimation may still contain noticeable phase lag. In contrast, an excessively large $\tau$ increases phase variation at high frequencies, amplifies noise, and reduces the stability margin during fast speed transitions. Therefore, $\tau$ should be selected within a moderate range:

$$0 < \tau < \tau_{\max}, \tag{27}$$

where $\tau_{\max}$ is determined according to the Bode response and time-domain verification. With this design, the all-pass filter provides the required phase compensation while maintaining sufficient phase margin and avoiding high-frequency oscillation.

## 3. Results

Experiments are carried out on a DTP-PMSM platform with a TI DSP28335, which sampling at 10 kHz, dead-time 2 µs, DC bus 320 V. The load motor operates in torque mode to provide accurate loading. The proposed MPRC with PC-IEID is compared with harmonic-suppression-free PI control, conventional MPC, and MPC-IEID. The experimental platform is shown in Figure 7.

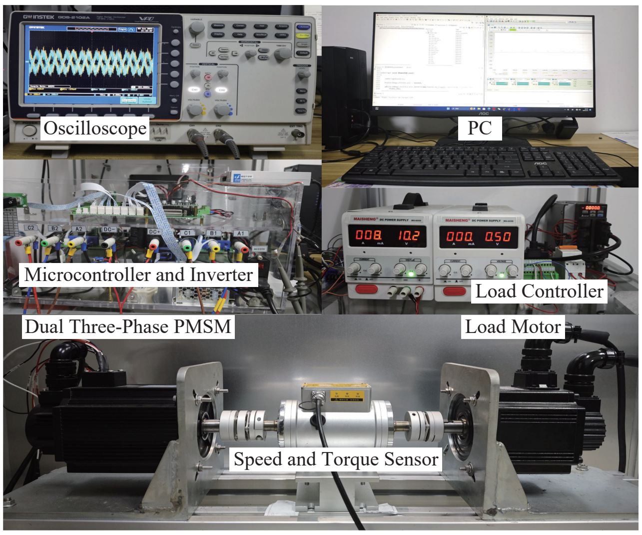


**Figure 7.** Experimental platform of DTP-PMSM.

In terms of periodic harmonic perturbation suppression in the dynamic-state, a speed step response experiment is evaluated by sequentially increasing the reference speed from 0 to 300 r/min, and then to 600 r/min. The experimental results are shown in Appendix A, as illustrated in Figure A1. Due to the decoupling of the subspaces based on vector space decomposition, the speed and q-axis current are almost unaffected by the different control methods, ensuring good dynamic response performance. However, harmonic disturbances become prominent in the $z_1$-$z_2$ space during dynamic processes. The PI and MPC control methods cannot effectively suppress these harmonic currents, whereas the MPC-IEID method allows for partial suppression during the dynamic response. The proposed MPRC with PC-IEID method demonstrates dynamic performance similar to the MPC-IEID method but achieves a further reduction in harmonic current amplitude, effectively suppressing harmonics during fast speed variations.

For steady-state performance, periodic harmonic disturbance suppression is evaluated under low-speed (300 r/min) and medium-high speed (1500 r/min) conditions, with both light (3 N·m) and heavy (9 N·m) loads. Under low-speed conditions, the PI and MPC controllers exhibit peak harmonic components in the frequency domain. The comparison of current sinusoidality and winding current balance performance of four control strategies in DTP-PMSMs under low-speed variable load conditions is shown in Figure A2. Correspondingly, the experimental results under medium-high speed (1500 r/min) with light and heavy load variation are illustrated in Figure A3. The proposed method still maintains excellent current sinusoidal quality and minimal harmonic fluctuation, verifying its effectiveness at medium-high speed operation. The comparison of the total harmonic distortion of phase A current at different speeds under low-load conditions is shown in Figure 8. Using the MPC-IEID method reduces the total harmonic distortion (THD) of the harmonic space currents to 6.52% for light loads and 4.31% for heavy loads. In comparison, the proposed MPRC with PC-IEID further reduces the THD to 5.33% and 3.98% for light and heavy loads, respectively. This demonstrates its effectiveness in targeting specific harmonic disturbances in the harmonic space and outperforming the MPC-IEID method when the load increases.

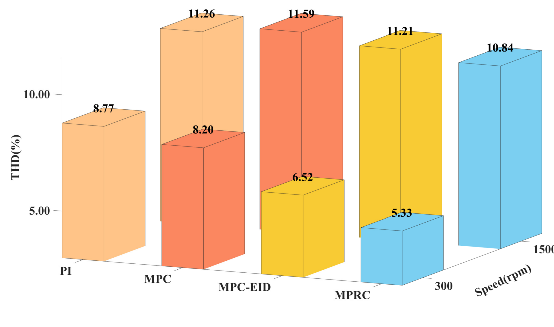


**Figure 8.** The THD comparison of A-phase current under low load with different speeds.

The comparison of A-phase current THD under heavy load at different speeds is presented in Figure 9. Under medium-high speed conditions, the THD values for the proposed method after a load increase are 4.61% and 10.84%, which are lower than those for the MPC-IEID method (4.96% and 11.21%). The MPC-IEID method shows limited suppression capability at higher speeds due to increased phase lag as the cutoff frequency approaches the disturbance fundamental frequency. Conversely, the proposed method effectively suppresses harmonic current disturbances at steady-state speeds by precisely adjusting the control inputs. Even with increased harmonics caused by lower carrier ratios and magnetic saturation under low load conditions, the reduction in THD values confirms the effectiveness of the MPRC with PC-IEID control method in suppressing harmonic distortions.

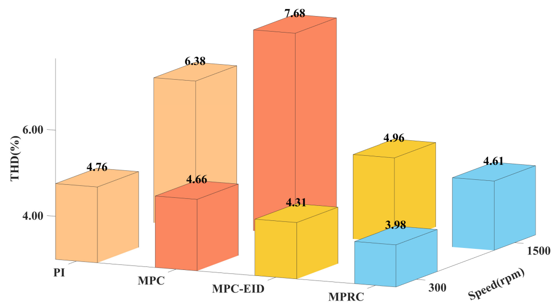


**Figure 9.** The THD comparison of A-phase current under heavy load with different speeds.

Finally, the system's robustness in handling non-periodic disturbances caused by parameter mismatches is evaluated under low-speed, low-load conditions (300 r/min, 3 N·m) with introduced errors in stator resistance and inductances, as shown in Figure 10. When only MPRC control is applied, the dq-axis currents experience significant fluctuations accompanied by an increase in $z_1$- and $z_2$-axis harmonic currents due to the parameter variations. However, when the PC-IEID is introduced, these fluctuations are significantly reduced as the disturbances caused by parameter mismatches are compensated. This indicates that the MPRC with PC-IEID control system demonstrates relatively high robustness under parameter mismatch conditions.

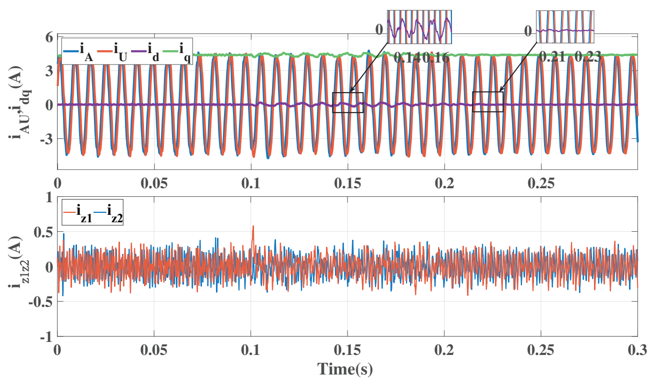


**Figure 10.** Experimental results of stator currents under inductance mismatch ($L_{es} = 0.9L_s$, $L_{ez} = 0.9L_z$) and resistance mismatch ($R_{es} = 0.9R_s$).

## 4. Discussion

The experimental results presented in the previous section validate the effectiveness of the proposed MPRC with PC-IEID control strategy for DTP-PMSM drives. This section provides a deeper analysis of these findings and their implications for harmonic suppression and system robustness.

### *4.1. Interpretation of Harmonic Suppression Performance*

The experimental verification confirms that the VSD achieves effective subspace decoupling, so speed and q-axis current are hardly affected by different control schemes. Harmonic disturbances mainly concentrate in the $z_1$-$z_2$ subspace. The proposed method outperforms conventional PI and MPC in harmonic suppression. Under low-speed conditions (300 r/min), the THD of MPRC with PC-IEID is 5.33% (light load) and 3.98% (heavy load), lower than 6.52% and 4.31% of MPC-IEID.

### *4.2. Addressing Limitations at Medium-High Speeds*

A critical observation in this study is the performance divergence at medium-high speeds (1500 r/min). The MPC-IEID method exhibited limited suppression capability at higher speeds, which can be attributed to the increased phase lag as the cutoff frequency of the filter approaches the disturbance fundamental frequency. In contrast, the proposed MPRC with PC-IEID effectively maintains suppression by precisely adjusting control inputs through its phase-compensated mechanism. This is highlighted by the lower THD values achieved by the proposed method (4.61% and 10.84%) compared to the MPC-IEID method (4.96% and 11.21%) under light and heavy load conditions at high speed. These results confirm that the proposed strategy successfully overcomes the phase lag issues inherent in traditional disturbance observers at high operating frequencies.

### *4.3. Robustness Against Parameter Mismatch*

The robustness of the control system is a vital factor for practical applications where motor parameters may vary. The experiments under stator resistance and inductance mismatch conditions (e.g., $L_{es} = 0.9L_s$ and $R_{es} = 0.9R_s$) reveal that while pure MPRC control suffers from significant current fluctuations and increased harmonic currents, the introduction of PC-IEID significantly mitigates these effects. By compensating for the disturbances caused by parameter variations, the system demonstrates high robustness. This confirms that the MPRC with PC-IEID not only targets periodic harmonic distortions but also effectively handles non-periodic disturbances caused by system modeling errors.

### *4.4. Summary of Contributions*

In summary, the experimental results demonstrate that the proposed method achieves a superior balance between dynamic response and steady-state precision. By integrating repetitive control with an improved equivalent input disturbance observer, the system effectively suppresses complex harmonic components that traditional predictive controllers cannot handle alone. The reduction in THD across various speeds and load conditions confirms the practical value of this approach for high-performance DTP-PMSM drive systems.

### 4.5. Study Limitations

Although the overall control performance has been improved, the proposed scheme still has certain limitations. The combined MPRC and PC-IEID architecture increases the computational load on the TMS320F28335 DSP, which operates at a 150 MHz main frequency with a clock cycle of approximately 6.667 ns, under a 10 kHz sampling frequency and a 100 µs control period. The control program comprises signal acquisition, MPRC computation, PC-IEID disturbance observation and phase compensation, SVPWM modulation, and hardware output, whose execution time statistics are reported in Table 1. Due to DSP floating-point characteristics and motor dynamic conditions, the per-cycle execution time exhibits slight fluctuations, multiple experiments show a maximum total execution time of 93.51 µs, which still leaves a safety margin at a 10 kHz sampling frequency. However, application to ultra-high-frequency sampling scenarios would demand further algorithm and code optimization. Furthermore, the ideal model also ignores real-world non-ideal characteristics such as winding asymmetry, inverter dead-time nonlinearity and magnetic saturation. These unmodeled dynamics bring extra disturbances and may adversely affect control accuracy. And we only tested steady-state performance and basic speed step responses here, the system's performance under complex speed variations is left for future research.

**Table 1.** Execution Time of Each Functional Module on TMS320F28335.

| Functional Module | Average Cycles | Maximum Cycles | Average Time (µs) | Maximum Time (µs) |
|---|---|---|---|---|
| Signal Acquisition | 2087 | 2381 | 13.91 | 15.87 |
| MPRC Computation | 4836 | 5264 | 32.24 | 35.10 |
| PC-IEID Observation & Phase Compensation | 4172 | 4589 | 27.81 | 30.59 |
| SVPWM & Hardware Output | 1589 | 1793 | 10.59 | 11.95 |
| Total Control Loop | — | — | 84.55 | 93.51 |

## 5. Conclusions

This paper proposes an MPRC method based on the IMP to suppress periodic harmonic disturbances in DTP-PMSM drives. Meanwhile, a PC-IEID observer is designed to mitigate non-periodic disturbances caused by parameter variations, which effectively reduces the adverse impact of such disturbances on the MPRC system and significantly enhances its robustness.

The periodic harmonic suppression is independently implemented in the $z_1$-$z_2$ subspace via VSD transformation, which ensures that the original dynamic control performance of the system remains intact while further minimizing motor copper losses and mechanical vibrations. The proposed approach also provides a practical parameter selection guideline for engineering implementation.

Comprehensive experimental results verify that the proposed method can effectively suppress both periodic harmonic and non-periodic disturbances in DTP-PMSM drives. Given the widespread adoption of VSD in multiphase motor control systems, this method can also be readily extended to other types of multiphase drives with decoupled harmonic subspaces.

## Author Contributions

L.G.: conceptualization (equal), data curation, investigation, design of MPRC and PC-IEID algorithms; W.L.: conceptualization (equal), software, writing—original draft preparation, experimental platform commissioning; J.W.: conceptualization (lead), supervision (overall research guidance), resources (experimental platform and funding support), validation (experimental scheme review), writing—reviewing and editing, project administration. All authors have read and agreed to the published version of the manuscript.

## Funding

This research was funded by the National Natural Science Foundation (NNSF) of China, grant number 62273306.

## Institutional Review Board Statement

Not applicable.

## Informed Consent Statement

Not applicable.

## Data Availability Statement

Data are contained within the article.

## Acknowledgments

The authors acknowledge the anonymous reviewers for their professional comments and suggestions.

## Conflicts of Interest

Le Gao is employed by Sany Heavy Machinery Company Ltd. This employment did not influence the design, conduct, or reporting of the study. The authors declare no other conflicts of interest.

## Use of AI and AI-Assisted Technologies

No AI tools were utilized for this paper.

## Appendix A

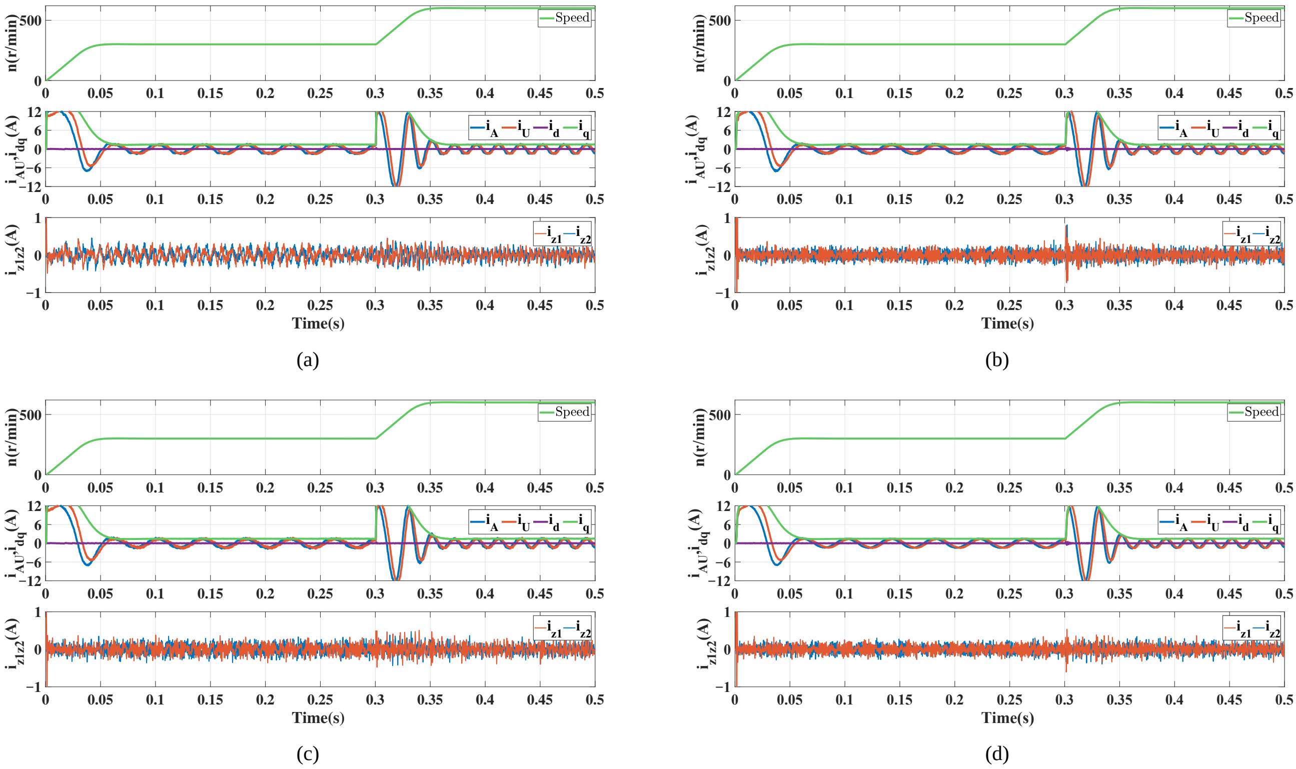


**Figure A1.** Comparison experiment results on speed step response. (**a**) PI; (**b**) MPC; (**c**) MPC−IEID; (**d**) MPRC with PC−IEID.

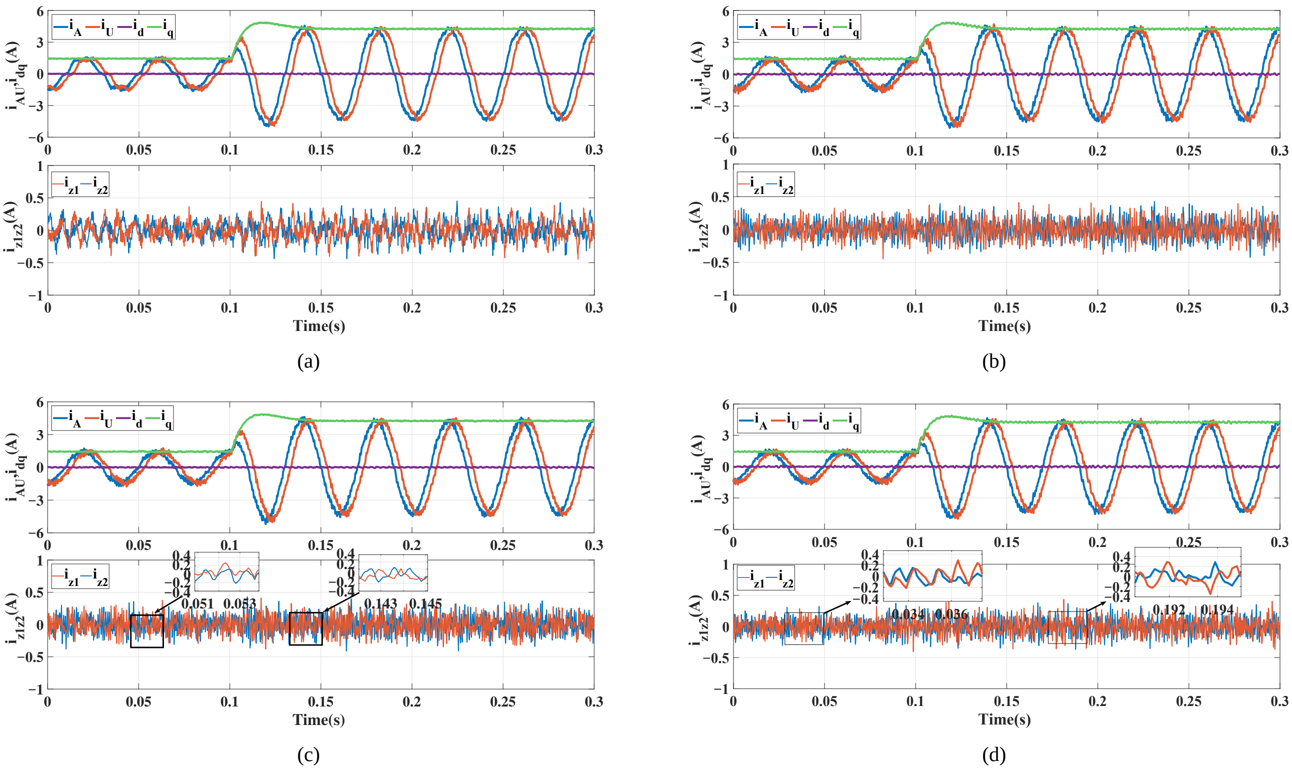


**Figure A2.** Experimental results of low-speed light load and heavy load (300 r/min, 3 N·m/9 N·m). (**a**) PI; (**b**) MPC; (**c**) MPC−IEID; (**d**) MPRC with PC−IEID.

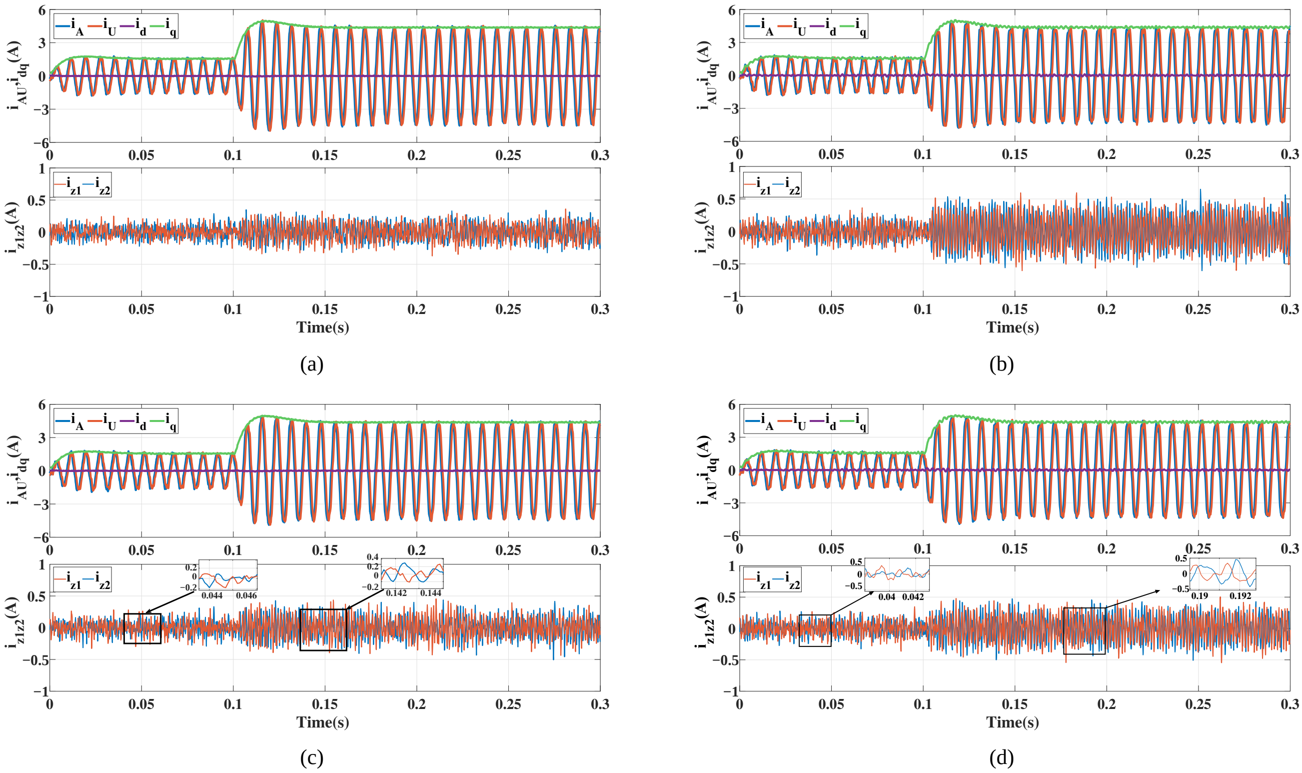


**Figure A3.** Experimental results of medium-high speed light load and heavy load (1500 r/min, 3 N·m/9 N·m). (**a**) PI; (**b**) MPC; (**c**) MPC−IEID; (**d**) MPRC with PC−IEID.

## References


1. Levi, E.; Barrero, F.; Duran, M.J. Multiphase machines and drives-revisited. *IEEE Trans. Ind. Electron.* **2016**, *63*, 429–432.
2. Che, H.S.; Levi, E.; Jones, M.; et al. Operation of a six-phase induction machine using series-connected machine-side converters. *IEEE Trans. Ind. Electron.* **2014**, *61*, 164–176.
3. Wang, X.; Wang, Z.; He, M.; et al. Fault-tolerant control of dual three-phase PMSM drives with minimized copper loss. *IEEE Trans. Power Electron.* **2021**, *36*, 12938–12953.
4. Ren, Y.; Zhu, Z.Q. Reduction of both harmonic current and torque ripple for dual three-phase permanent-magnet synchronous machine using modified switching-table-based direct torque control. *IEEE Trans. Ind. Electron.* **2015**, *62*, 6671–6683.
5. Zhao, Y.; Lipo, T. Space vector PWM control of dual three-phase induction machine using vector space decomposition. *IEEE Trans. Ind. Appl.* **1995**, *31*, 1100–1109.
6. Cui, J.; Tao, T.; Zhao, W. Optimized control set model predictive control for dual three-phase PMSM with minimum error duty cycle regulation. *IEEE Trans. Power Electron.* **2024**, *39*, 1319–1332.
7. Hadiouche, D.; Baghli, L.; Rezzoug, A. Space-vector PWM techniques for dual three-phase AC machine: analysis, performance evaluation, and DSP implementation. *IEEE Trans. Ind. Appl.* **2006**, *42*, 1112–1122.
8. Liu, X.; Wang, J.; Gao, X.; et al. Continuous control set predictive speed control of SPMSM drives with short prediction horizon. *IEEE Trans. Power Electron.* **2022**, *37*, 10166–10177.
9. Liu, S.; Liu, C. Direct harmonic current control scheme for dual three-phase PMSM drive system. *IEEE Trans. Power Electron.* **2021**, *36*, 11647–11657.
10. Zhang, Z.; Wang, Z.; Wei, X.; et al. Space-vector-optimized predictive control for dual three-phase PMSM with quick current response. *IEEE Trans. Power Electron.* **2022**, *37*, 4453–4462.
11. Luo, Y.; Liu, C. A simplified model predictive control for a dual three-phase PMSM with reduced harmonic currents. *IEEE Trans. Ind. Electron.* **2018**, *65*, 9079–9089.
12. Lim, C.S.; Lee, S.S.; Levi, E. Continuous-control-set model predictive current control of asymmetrical six-phase drives considering system nonidealities. *IEEE Trans. Ind. Electron.* **2023**, *70*, 7615–7626.
13. Xu, Y.; Zheng, B.; Wang, G.; et al. Current harmonic suppression in dual three-phase permanent magnet synchronous machine with extended state observer. *IEEE Trans. Power Electron.* **2020**, *35*, 12166–12180.
14. Cao, H.; Deng, Y.; Liu, J.; et al. Improved deadbeat predictive current control of PMSM drives with repetitive control-based disturbance correction observer. *IEEE Trans. Power Electron.* **2025**, *40*, 801–812.
15. Mei, Q.; She, J.; Long, F.; et al. Performance enhancement for systems with disturbances and measurement noise by modified equivalent-input-disturbance approach. *IEEE Trans. Ind. Electron.* **2024**, *71*, 14516–14525.
16. Du, Y.; Cao, W.; She, J.; et al. Disturbance rejection and control system design using improved equivalent input disturbance approach. *IEEE Trans. Ind. Electron.* **2020**, *67*, 3013–3023.
17. Wang, J.; Chen, L.; Xu, Q. Disturbance estimation-based robust model predictive position tracking control for magnetic levitation system. *IEEE/ASME Trans. Mechatron.* **2022**, *27*, 81–92.
18. Wang, J.; Wang, F.; Wang, G.; et al. Generalized proportional integral observer based robust finite control set predictive current control for induction motor systems with time-varying disturbances. *IEEE Trans. Ind. Inform.* **2018**, *14*, 4159–4168.

19. Karttunen, J.; Kallio, S.; Peltoniemi, P.; et al. Current harmonic compensation in dual three-phase PMSMs using a disturbance observer. *IEEE Trans. Ind. Electron.* **2016**, *63*, 583–594.
20. Stanković, M.R.; Rapaić, M.R.; Manojlović, S.M.; et al. Optimised active disturbance rejection motion control with resonant extended state observer. *Int. J. Control* **2019**, *92*, 1815–1826.
21. Zhang, G.; Zhao, Q.; Ye, Y.; et al. Feedforward repetitive control for grid-tied inverters in microgrids: Analysis, design, and verification. *IEEE Trans. Ind. Electron.* **2024**, *71*, 11239–11249.
22. Lu, W.; Zhou, K.; Wang, D.; et al. A generic digital nk±m-order harmonic repetitive control scheme for PWM converters. *IEEE Trans. Ind. Electron.* **2014**, *61*, 1516–1527.
23. Tian, M.; Wang, B.; Yu, Y.; et al. Discrete-time repetitive control-based ADRC for current loop disturbances suppression of PMSM drives. *IEEE Trans. Ind. Inform.* **2022**, *18*, 3138–3149.
24. Lunardi, A.; Conde, E.; Assis, J.; et al. Repetitive predictive control for current control of grid-connected inverter under distorted voltage conditions. *IEEE Access* **2022**, *10*, 16931–16941.
25. Liu, Y.; Cheng, S.; Ning, B.; et al. Robust model predictive control with simplified repetitive control for electrical machine drives. *IEEE Trans. Power Electron.* **2019**, *34*, 4524–4535.
26. Guo, L.; Xu, J.; Wu, S.; et al. Analysis and design of dual three-phase fractional-slot permanent magnet motor with low space harmonic. *IEEE Trans. Magn.* **2022**, *58*, 8100112.
27. Dajaku, G.; Xie, W.; Gerling, D. Reduction of low space harmonics for the fractional slot concentrated windings using a novel stator design. *IEEE Trans. Magn.* **2014**, *50*, 8201012.
28. Abdel-Khalik, A.S.; Ahmed, S.; Massoud, A.M. Low space harmonics cancelation in double-layer fractional slot winding using dual multiphase winding. *IEEE Trans. Magn.* **2015**, *51*, 8104710.
29. Sun, W.; Gao, J.; Liu, X.; et al. Inverter nonlinear error compensation using feedback gains and self-tuning estimated current error in adaptive full-order observer. *IEEE Trans. Ind. Appl.* **2016**, *52*, 472–482.